Short-time dynamics of a tracer in an ideal gas

Fumiaki Nakai [1], Yuichi Masubuchi [2], and Takashi Uneyama [2]

[1]*Department of Materials Physics, Graduate School of Engineering, Nagoya University, Furo-cho, Chikusa, Nagoya 464-8603, Japan*
[2]*Center for Computational Science, Graduate School of Engineering, Nagoya University, Furo-cho, Chikusa, Nagoya 464-8603, Japan*

A small tagged particle immersed in a fluid exhibits Brownian motion and diffuses on a long timescale. Meanwhile, on a short timescale, the dynamics of the tagged particle cannot be simply described by the usual generalized Langevin equation with Gaussian noise, since the number of collisions between the tagged particle and fluid particles is rather small. On such a timescale, we should explicitly consider individual collision events between the tagged particle and the surrounding fluid particles. In this study we analyze the short-time dynamics of a tagged particle in an ideal gas, where we do not have static or hydrodynamic correlations between fluid particles. We perform event-driven hard-sphere simulations and show that the short-time dynamics of the tagged particle is correlated even under such an idealized situation. Namely, the velocity autocorrelation function becomes negative when the tagged particle is relatively light and the fluid density is relatively high. This result can be attributed to the dynamical correlation between collision events. To investigate the physical mechanism which causes the dynamical correlation, we analyze the correlation between successive collision events. We find that the tagged particle can collide with the same ideal-gas particle several times and such collisions cause a strong dynamical correlation for the velocity.

I. INTRODUCTION

A particle immersed in a fluid exhibits random motion, which is widely known as Brownian motion [1]. The Brownian motion originates from the interaction between a tagged particle (tracer) and the particles which compose the surrounding fluid (fluid particles). In principle, the dynamics of the tracer is deterministic because the full system, which consists of the tracer and the fluid particles, obeys the Hamiltonian dynamics. However, if we observe only the tracer, the dynamics looks stochastic (at least apparently).

For a description of such stochastic dynamics of the tracer, the generalized Langevin equation (GLE) [2,3] has been employed in many cases. The GLE is a stochastic differential equation which incorporates the memory effect (memory kernel) and random noise. The properties of the memory kernel and the random noise reflect the statistical properties of the surrounding fluid. Formally, the projection operator method [4] gives an expression for the memory kernel and the noise is related to the memory kernel via the fluctuation-dissipation relation. The dynamic equation for the tracer is given as

$$M\frac{d^2\boldsymbol{r}(t)}{dt^2} = -\int_{-\infty}^{t} dt' K(t-t')\frac{d\boldsymbol{r}(t')}{dt'} + \boldsymbol{\xi}(t), \quad (1)$$

where $\boldsymbol{r}$ and M are the position and mass of the tracer, $K(t)$ is the memory kernel, and $\boldsymbol{\xi}(t)$ is the random noise. The random noise satisfies

$$\langle \boldsymbol{\xi}(t)\rangle = 0, \quad \langle \boldsymbol{\xi}(t)\boldsymbol{\xi}(t')\rangle = k_B T K(|t-t'|)\mathbf{1}, \quad (2)$$

where $\langle \cdots \rangle$ represents the statistical average, k_B is the Boltzmann constant, T is the temperature, and $\mathbf{1}$ is the unit tensor.

The projection operator formalism does not tell us the full properties of the noise $\boldsymbol{\xi}(t)$. It gives only the first and second moments as Eq. (2). Therefore, in many practical cases, the noise is assumed to be Gaussian. Then the dynamic equation for the tracer is fully specified and can be analytically solved [5]. Such a GLE with Gaussian noise is utilized to analyze various experimental data [6–10]. The diffusion of the tracer can also be directly studied by molecular dynamics simulations. Recently, the memory kernels for some systems have been calculated precisely from molecular dynamics simulations [11,12]. For example, the power-law-type long-time tail, which originates from hydrodynamic modes, was reported for a Lennard-Jones fluid [11]. It should be noted that, in most cases, a tracer is assumed to be large and heavy [13]. However, in some cases, a tracer could be rather small and light. For example, if we interpret a molecule which is dissolved in a fluid as a tracer, the tracer size is comparable to the fluid particles and the mass of the tracer is also comparable to that of a fluid particle. (For example, if we consider a mixture system which consists of isotopes and interpret a light species as a tracer, the tracer mass can be slightly smaller (or larger) than unity [14].) The dynamics of a tracer particle can be experimentally measured, for example, by scattering, and we need to describe the dynamics of the tracer particle to analyze the experimental data.

Here we emphasize that the Gaussian noise approximation is not justified *a priori*. Naively, we expect that the approximation is reasonable because the noise would be Gaussian as a result of the many accumulated forces due to the collisions of surrounding fluid particles. As long as the number of collisions is sufficiently large, the average force will converge to a

Gaussian noise by the central limit theorem. Conversely, when the number of collisions is insufficient, the Gaussian noise approximation does not work properly. Such a situation can be realized when we consider the dynamics of a single tagged particle in a dilute gas. The Gaussianity of the noise can be evaluated via the Gaussianity of the displacement, since the displacement is a linear combination of the noise [by Eq. (1)]. For instance, Yamaguchi and Kimura [15] investigated the dynamics of a single hard sphere in a dilute hard-sphere gas. They reported that the distribution function for the displacement is non-Gaussian on a short timescale. We should be careful when we employ the Gaussian noise approximation.

The tracer dynamics for the short timescale in a dilute fluid can be described, for example, by the kinetic theory of gases [16]. To illustrate the dynamics with a small number of collisions, we should consider the individual collision events explicitly. Then we expect that the dynamics would be modeled by the sequence of collision events. Burshtein and Krongauz [17] modeled the dynamics of a tracer in a hard-sphere fluid as a sequence of collision events. They assumed simple statistics for the collision events (the statistical distributions of the waiting time between successive collisions and the velocity change distribution are decoupled and given as simple hypothetical forms) and calculated dynamical quantities such as the velocity autocorrelation function (VAC). Their model can successfully reproduce some dynamical properties. However, we note that the statistics employed would be a matter of further discussion. We expect that the statistics depend rather strongly on the fluid density. When the fluid is dilute, the collisions are statistically almost independent [16]. Some assumptions in the Burshtein-Krongauz model will be justified in such a case. However, when the fluid is rather dense, the situation becomes very complex. In a dense hard-sphere fluid [18,19], the statistics of collisions would depend on various factors. For example, they can be related to the structure of the fluid. Recently, Mizuta *et al.* [20] performed a series of molecular dynamics simulations for a fullerene particle immersed in liquid argon. They reported that the dynamics of fullerene particles is affected by both the hydrodynamics and structure of the fluid. Although their result is interesting, it seems difficult to quantitatively separate the contributions of individual factors.

The statistics of collision events can also depend on the mass of the tracer. For a collision between two hard spheres, the velocities of the spheres after the collision depend on the velocities before the collision and the masses of the two hard spheres. The collision statistics depend on the cross section of the collision and the relative velocity. For the collision between a tracer particle and a fluid particle, the statistics of the relative velocity depend on the masses of the tracer and the fluid particle. Also, the momentum exchange between the tracer and the ideal-gas particle depends on the mass ratio. Then, if the mass of the tracer is changed, the collision statistics would change (by the change of the relative velocity distribution). If the tracer mass is sufficiently larger than the fluid molecule mass, the momentum of the tracer will not be largely affected by a single collision. However, if the tracer mass is relatively small, the momentum largely changes even by a single collision and consequently the backreflection and the negative velocity autocorrelation of the tracer can occur [19,21]. The statistics of the collision events would not be

simple in this case. Such collision statistics can be naturally handled by utilizing the methods developed in the kinetic theory of gases [16,22], instead of the GLE. We can describe the dynamics by the Boltzmann equation or by the Fokker-Planck equation and then employ some collision statistics to calculate the dynamical quantities such as the velocity autocorrelation. For dilute gases, we may reasonably assume that collisions are statistically independent. Then the collision distribution can be described by the Poisson process; some dynamical quantities behave qualitatively different from the GLE with the Gaussian noise approximation. For example, the mass dependence of the diffusion coefficient can be explained by the kinetic theory of gases. If the gas density is relatively high, however, the description by the kinetic theory of gases becomes nontrivial. The Burshtein-Krongauz model would be interpreted as a phenomenological extension of the kinetic theory to a relatively dense system. An extension of the GLE by combining non-Gaussian-type processes which mimic collisions has also been proposed [23,24]. However, the microscopic origin of the negative velocity correlation has not been fully clarified yet.

In this paper we investigate the dynamics of the tracer particle on a short timescale, from the viewpoint of collision events. As we mentioned, the statistics of collision events and the short-time dynamics of the tracer depend on both the fluid density and the tracer mass. They are also affected by several different factors such as the fluid structure and the hydrodynamic interaction. To eliminate such factors other than the fluid density and the tracer mass, we consider systems where fluid particles do not interact with each other (the ideal gas). We investigate the dynamics of the tracer in the ideal gas by the hard-sphere simulations. We perform a series of simulations with various parameter sets. We find that the tracer exhibits a rather complex dynamics on the short timescale, even by such an idealized and simplified model. We analyze the dynamics of the tracer on the basis of the collision-type dynamics by Burshtein and Krongauz [17]. We show that the correlation between sequential collisions is important in describing the short-time dynamics of the tracer.

II. MODEL AND METHOD

We consider the dynamics of a tracer immersed in an ideal gas by a numerical simulation. In this work we use the term "ideal gas" to mean a gas composed of point masses which do not interact with each other at all. The point masses do not exchange their momenta via collisions. The tracer collides with the ideal-gas particles whereas the ideal-gas particles do not collide with each other. We model the tracer as a hard-sphere particle and employ the standard hard-sphere simulation method [25]. Both the tracer and ideal-gas particles move ballistically until they collide. The velocities of the tracer and ideal-gas particles instantaneously change when they collide.

We consider a single tracer particle and N ideal-gas particles in the cubic simulation box with periodic boundary conditions. We set the number of ideal-gas particles as $N = 10^5$ for all the simulations. We express the masses of the tracer and ideal-gas particles as M and m, respectively, the size of the tracer as σ (the size of the ideal-gas particles is 0), the temperature of the system as T, and the number density

of the ideal-gas particles as ρ. [Here the particle density is related to the system volume $\mathcal{V}$ as $\rho = N/(\mathcal{V} - \pi\sigma^3/6)$.] We employ dimensionless units where the units of energy, mass, and length are $k_B T$ (k_B is the Boltzmann constant), m, and σ, respectively. In dimensionless units, the system can be characterized only by two parameters: M and ρ. We vary the density ρ in the range from 10^{-2} to 10^3 and the mass M in the range from 10^{-2} to 10^3.

The initial state of the simulation is generated as follows. The tracer particle is located at the box center and the ideal-gas particles are dispersed randomly in the box. (The position of a newly generated ideal-gas particle should not overlap with the tracer.) The initial velocities of the tracer and ideal-gas particles are sampled from the Maxwell-Boltzmann distribution. To prevent the center of mass of the system from drifting, we subtract the velocity of the center of mass from all the particles in the system. Then the velocities of the particles are rescaled to reduce the average kinetic energy to $3/2$. Since the momentum is conserved in the hard-sphere simulation, the center of mass does not move during a simulation. After the initial state is generated, we evolve the system by using the established procedure for the hard-sphere simulation [25].

Although the hard-sphere simulation itself is rather simple and clear, we should be careful about the handling of the images due to the periodic boundary condition. In this simulation, the mean free path of the tracer is long and this leads to unexpected overlaps between the tracer and images of ideal-gas particles. To avoid such overlaps, we perform the simulations as follows.

1. We generate the initial state.

2. We find the ideal-gas particle (the target particle), which collides with the tracer judging from their positions and velocities. The waiting time for the collision of this particle is Δt_1.

3. We find the ideal-gas particle, which has a maximum velocity relative to the tracer along the axis of the simulation box. From the maximum relative velocity V_{max}, we obtain the minimum time of collision of the image particle with the tracer as $\Delta t_2 = (L - \sigma)/2V_{max}$, where L ($= \mathcal{V}^{1/3}$) is the box length.

4. If $\Delta t_2 < \Delta t_1$, we update the position of all particles by the step size Δt_2, then proceed to $t \rightarrow t + \Delta t_2$, and repeat the update unless $\Delta t_1 \leqslant \Delta t_2$. When $\Delta t_1 \leqslant \Delta t_2$ is satisfied, we update the position of all particles by the step size Δt_1 and then proceed to $t \rightarrow t + \Delta t_1$ to attain the collision.

5. We update the velocity of the tracer and the target particle according to the collision.

6. We repeat steps 2-5 until 10×10^6 collisions are attained.

From the trajectories of the tracer, we calculate several dynamical quantities: the mean-square displacement (MSD), the non-Gaussian parameter (NGP) [26], and the velocity autocorrelation function defined, respectively, as

$$g(t) \equiv \langle \Delta \boldsymbol{r}^2(t) \rangle, \tag{3}$$

$$\alpha(t) \equiv \frac{3\langle \Delta \boldsymbol{r}^4(t) \rangle}{5\langle \Delta \boldsymbol{r}^2(t) \rangle^2} - 1, \tag{4}$$

$$C(t) \equiv \frac{\langle \boldsymbol{V}(t) \cdot \boldsymbol{V}(0) \rangle}{\langle \boldsymbol{V}^2 \rangle}. \tag{5}$$

Here $\Delta \boldsymbol{r}(t) \equiv \boldsymbol{r}(t) - \boldsymbol{r}(0)$ is the displacement of the tracer, $\boldsymbol{V}(t)$ is the velocity of the tracer and $\langle \cdots \rangle$ represents the statistical average. We also calculate a few quantities which characterize the change of the tracer velocity by collisions. They will be introduced later.

Before we show the simulation results; here we briefly comment on the effect of the system size on the simulation results. In our model, the ideal-gas particles can change their velocities only via the collision with the tracer. Thus the relaxation time for the velocity of an ideal-gas particle becomes very long and it depends on the system size. One may consider that the velocity distribution of the ideal-gas particles deviate from the equilibrium distribution. Also, one may suspect that the dynamics of the tracer strongly depends on the system size. Fortunately, as far as we examined, the velocities of the ideal-gas particles obey the equilibrium Maxwell-Boltzmann distribution. Some dynamical quantities of the tracer, such as the MSD and VAC, do not show a measurable system size dependence (unless the system size is too small and comparable to the tracer size). Therefore, we conclude that the system-size dependence for simulation results can be safely neglected (at least for the analysis shown below).

III. RESULTS

Figure 1(a) shows the mass dependence of the MSD for an ideal-gas density of $\rho = 1$. In a short-time region, the ballistic behavior $\langle \Delta \boldsymbol{r}^2(t) \rangle \propto t^2$ is observed and the MSD decreases as M increases. This behavior is consistent with the fact that the average absolute value of velocity decreases as M increases. In a long-time region, diffusive behavior $\langle \Delta \boldsymbol{r}^2(t) \rangle \propto t$ is observed and the MSD decreases as M increases. This result means that the diffusion coefficient of the tracer depends on M. One may argue that the M dependence is counterintuitive because the GLE (1) predicts that the inertia term does not contribute to the long-time dynamics. However, from the viewpoint of the kinetic theory of gases, the diffusion coefficient can depend on the mass [16]. A similar behavior has been reported for the motion of a tracer in Lennard-Jones fluids [27,28] and hard-sphere fluids [21]. Nevertheless, in this work we do not discuss the M dependence of the diffusion coefficient.

Figure 1(b) shows the M dependence of the NGP. The parameters are the same as in Fig. 1(a). The NGP increases with time in the ballistic regime, exhibits a peak in the transitional regime, and decays in the diffusive regime. The peak increases as M decreases. This result means that the statistics of the displacement is non-Gaussian except in the diffusive regime when M is small. The non-Gaussian behavior is observed in various systems and often attributed to the heterogeneity of the environment. For example, the glass forming liquids [29] and polymer solutions [30] work as heterogeneous environments for a tracer. However, in our system, the ideal-gas particles never have the structures and thus the non-Gaussian behavior cannot be attributed to the heterogeneity of the environment. Therefore, we consider the non-Gaussian behavior to have kinetic origin. In our system, the tracer dynamics is affected only by the collisions and the non-Gaussian behavior can be attributed to the properties of collisions. (Yamaguchi
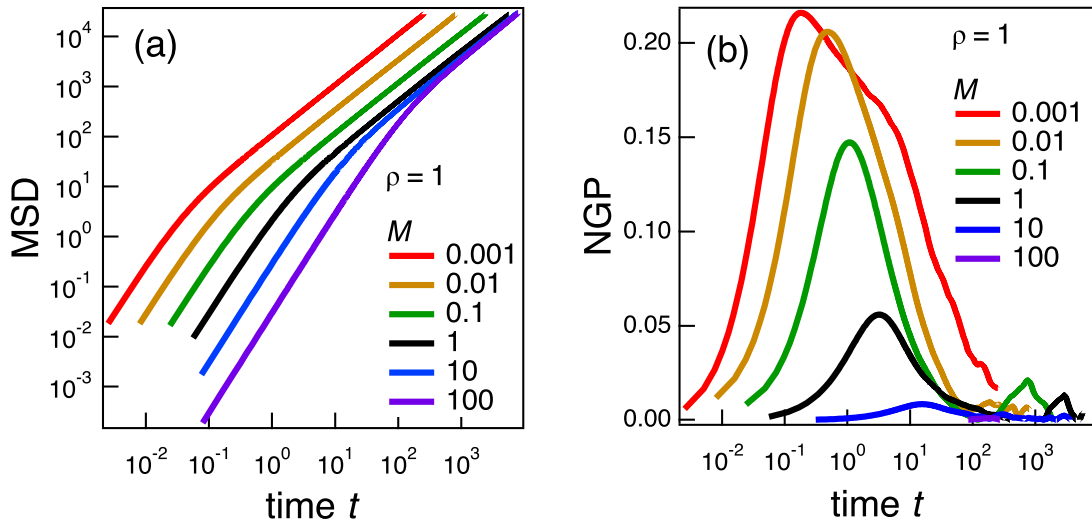
FIG. 1. The (a) MSD and (b) NGP of a tracer in an ideal gas for various M. The density of the ideal gas is $\rho = 1$.

and and Kimura also reported similar non-Gaussian behavior for a dilute hard-sphere fluid [15].)

Figure 2 shows the ρ dependence of the MSD and NGP with a constant mass of the tracer ($M = 1$). We observe that the MSD collapses onto a single curve in the ballistic region. The MSD deviates from the ballistic behavior to the diffusive behavior and the crossover time decreases as ρ increases. This ρ dependence is due to the change of the mean free path. In Fig. 1 we observe a non-negligible peak for the NGP. The peak value of the NGP is almost constant for $\rho \leqslant 1$, whereas the value increases slightly as ρ increases for $\rho \geqslant 1$. Although such an increase of the NGP against ρ is commonly observed for liquids with heterogeneous structures [31], we have no heterogeneity in our model, as mentioned above.

From the mass and density dependence shown above, we conclude that the dynamics of the tracer qualitatively depends on the mass and the density. If the mass is large ($M \gtrsim 1$), the dynamics of the particle can be reasonably described as the Gaussian process. (The GLE with the Gaussian noise

approximation is reasonable.) If the density is low ($\rho \lesssim 1$), the dynamics of the tracer can be expressed by the ballistic motion and collisions (as the standard kinetic theory of gases [16]). However, if the mass is small and the density is high ($M \lesssim 1$ and $\rho \gtrsim 1$), the dynamics seems not to be expressed as a simple and intuitive model. We consider that this is caused by the "dynamic" correlation. (In our system, the fluid has no static structure since it is an ideal gas.) Our result suggests that the dynamic correlation solely gives such an apparently counterintuitive behavior. A simple interpretation is that something like a "cage" would be dynamically formed and the tracer effectively experiences confinement on the short timescale. However, this behavior is not trivial, and to investigate it in detail we performed some additional simulations for several parameter sets for $M \lesssim 1$ and $\rho \gtrsim 1$.

Figure 3 shows the MSD and NGP for several different parameter sets. From Fig. 3(a) we find that the MSD shows unexpected behavior for $M = 0.01$ and $\rho = 100$. Namely, the MSD does not show the plain crossover from ballistic
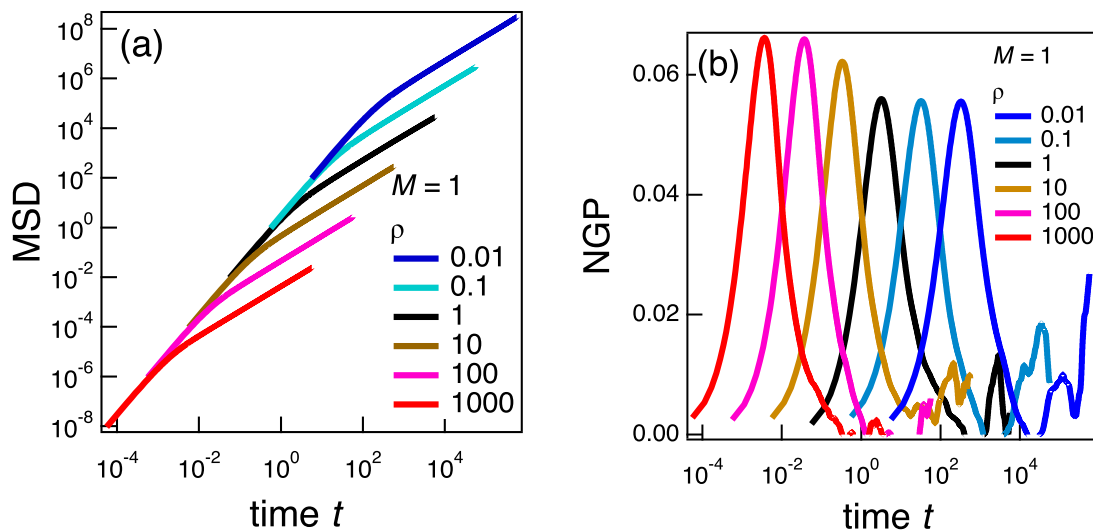

FIG. 2. The (a) MSD and (b) NGP of a tracer in an ideal gas for various ρ. The mass of the tracer is $M = 1$.
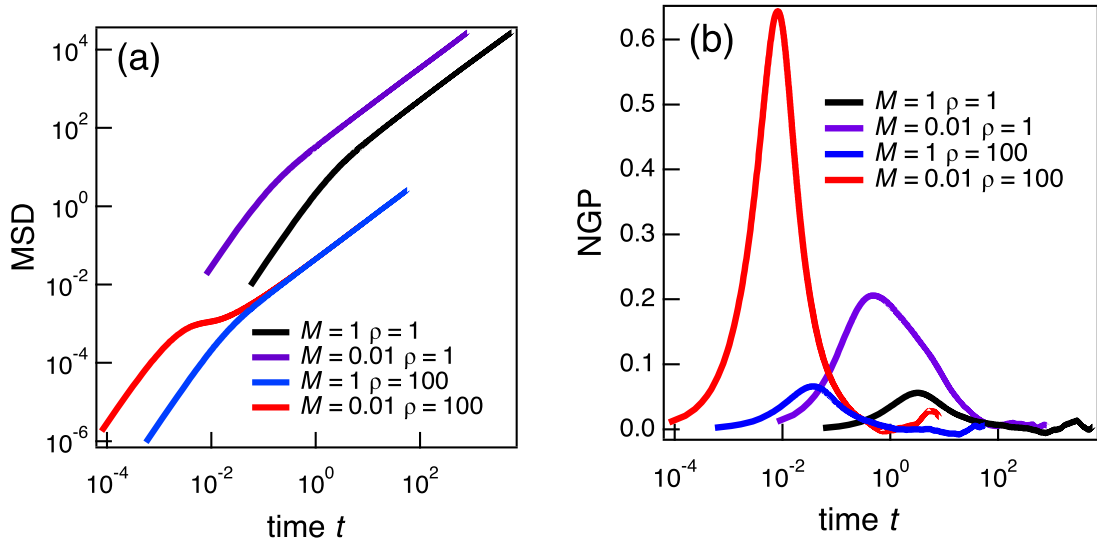
FIG. 3. The (a) MSD and (b) NGP of a tracer for several sets of mass M and an ideal-gas density ρ.

to diffusive behavior and we observe an intermediate sub-diffusive region between the ballistic and diffusive regions. Similar behavior of the MSD has been reported for several systems such as glass forming liquids and polymer solutions [32,33]. Although the data are not explicitly presented, similar behavior has also been reported for the multi particle collision dynamics (MPCD) type of model [34]. In Fig. 3(b) we observe a strong peak of the NGP for $M = 0.01$ and $\rho = 100$. [Intuitively, the peak time for the NGP (t_{peak}) corresponds to the relaxation time of the tracer velocity. This interpretation seems to be consistent with the MSD data. The MSD exhibits ballistic behavior for $t \lesssim t_{peak}$ and diffusive behavior for $t \gtrsim t_{peak}$.] Thus demonstrated, we confirm that our system exhibits nontrivial dynamical behavior for small M and high ρ. These results seem not to be simply described by the GLE or the kinetic theory of gases. Questions naturally arise: What is the origin of such nontrivial behavior? How can we describe the dynamics?

Here we recall that our simulation model is a collision-driven hard-sphere molecular dynamics model. In our model, the tracer moves ballistically and the velocity changes only through collisions with the ideal-gas particles. Therefore, it would be reasonable for us to concentrate on the velocity of the tracer. Figure 4 shows the VAC of a tracer particle for the same parameter sets as in Fig. 3. For the case of $M = 0.01$ and $\rho = 100$, the VAC becomes negative in the intermediate-time region. The negative correlation in the VAC means that the tracer is effectively reflected back by collisions (the backreflection). A negative VAC is usually attributed to the strong static and dynamic correlations between fluid particles. However, in our system, the ideal-gas particles do not have static and dynamic correlations and thus we cannot attribute the negative VAC to the correlations between fluid particles. A possible intuitive interpretation is as follows. If the mass of the tracer is small, the tracer has a high velocity compared with the surrounding ideal-gas particles. Also, due to the large mass contrast, the momentum of an ideal-gas particle is almost unaffected when the tracer and the ideal-gas particle collide. Thus, we may interpret the ideal-gas particles as almost fixed

obstacles. Under such a situation, the backreflection behavior may occur. Meanwhile, we should notice that the effect of the backreflection becomes especially strong when the density is high. To clarify the short-time dynamics, therefore, we should analyze the collisions in detail. In addition to the short-time dynamics, the long-time dynamics is important for some analyses. The VAC typically exhibits a so-called long-time tail in the long-time region. In our simulation results, however, a power-law-type long-time tail is not clearly observed, at least in the timescale examined. (We may observe the long-time tail on a very long timescale, but it is beyond the scope of this work and thus we do not consider the long-time region in what follows.)

Burshtein and Krongauz [17] considered a similar negative velocity correlation in hard-sphere fluids. They analyzed the dynamics of a hard sphere carefully and proposed a simple model which describes the motion of a hard sphere. They
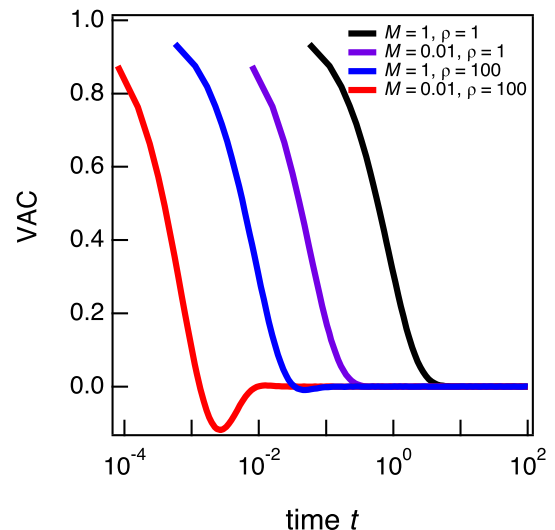

FIG. 4. The VAC of a tracer for several sets of mass and ideal-gas density. The parameters are the same as in Fig. 3.
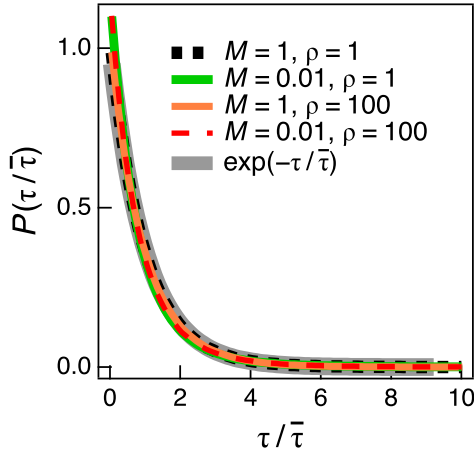
FIG. 5. Waiting-time distribution function $P(\tau)$ for different values of the mass M and ideal-gas density ρ. The waiting time τ is normalized by the average $\bar{\tau}$ as $\tau/\bar{\tau}$. For comparison, the exponential distribution $P(\tau) = (1/\bar{\tau}) \exp(-\tau/\bar{\tau})$ is also plotted.

modeled a process as a sequence of collision events, which we may interpret as a renewal process. They assumed that the time interval between two successive collisions is sampled from a waiting-time distribution $P(\tau)$ and there is no correlation between successive waiting times. They also assumed that the velocity of the hard sphere is stochastically changed from V to V' and the new velocity V' is sampled from the velocity distribution $P(V'|V)$. Their model claims that the negative velocity correlation can emerge if both of the following conditions are satisfied: (a) The waiting-time distribution $P(\tau)$ is not an exponential distribution and (b) the average velocity after a collision is negatively correlated to the velocity before the collision, $\langle V' \cdot V \rangle < 0$. Although their model seems plausible, some assumptions in their model cannot be fully justified. Thus we investigate the statistics of collisions in our simulations below.

Figure 5 shows the waiting-time distribution between two successive collision events. In this work we define the waiting time as the time interval between two successive collision events. (We do not distinguish whether or not the tracer collides with the same ideal-gas particle.) The waiting time τ is normalized by the average waiting time $\bar{\tau} \equiv \int d\tau\, \tau P(\tau)$. We observe that the distribution function for the normalized waiting time is almost independent of M and ρ. Moreover, the waiting-time distribution can be reasonably fit to the exponential distribution. Naively, the exponential waiting-time distribution means that the collision events are statistically independent. Thus this result implies the Poisson distribution for the number of collisions during a finite-time period. However, this naive argument is physically not fully justified. This is because the statistics of the waiting time generally depend on the tracer velocity. The observed waiting-time distribution should be interpreted as the average waiting-time distribution over the tracer velocity. This average waiting-time distribution seems to be well described by the exponential distribution. (We show the calculations for the waiting-time distributions in Appendix A.) Anyway, assumption (a) is not satisfied. According to the Burshtein-Krongauz model, if the waiting-time distribution is exponential, then the VAC is always positive.

Clearly, this is not consistent with our simulation result in Fig. 4. We expect that some assumptions by Burshtein and Krongauz would not be valid (at least for our system). We will discuss the statistical properties of collisions in detail in the next section.

IV. DISCUSSION

A. Gaussianity

In this section we discuss the Gaussianity of the dynamics of the tracer. Our simulation results (Figs. 1–3) show that the tracer exhibits non-Gaussian behavior even if the surrounding fluid is an ideal gas. The NGP strongly depends on the tracer mass M, and if M is sufficiently large, the NGP becomes small. Therefore, if M is sufficiently large, the dynamics of the tracer can be reasonably described by a Gaussian process. For such a case, the GLE with Gaussian noise can be utilized.

As we mentioned, the GLE with Gaussian noise has been widely employed to analyze experimental data. However, our results imply that the application of the GLE may not be fully justified in some cases. Here we discuss the validity of the GLE for some experimental systems. Recent progress of experimental techniques has enabled us to experimentally measure the short-time ballistic motion of a tracer particle [8,10]. Li *et al.* [8] investigated the dynamics of 3-μm beads in dilute gases (2.75 and 99.8 kPa) on the microsecond scale. The mass of the tracer is about 10^{-10} g, whereas the mass of the gas molecule is about 10^{-23} g. Clearly, the mass ratio is very large (about 10^{13}) and thus we expect that the tracer dynamics is reasonably described by the GLE. Note that the memory effect is negligible in this system and thus the GLE reduces to a simple Langevin equation. Huang *et al.* [10] measured the dynamics of a tracer in a fluid. Although the fluid density is much larger than in the experiments by Li *et al.*, the mass ratio is estimated to be the same order as that of Li *et al.* Therefore, we conclude that for typical experimental conditions for the short-time dynamics of a tracer particle, the GLE (or the Langevin equation) with Gaussian noise can be safely employed.

However, the argument above does not fully justify the use of the Langevin equation to analyze the other experimental data. The Langevin equation is utilized for various analyses of experimental data, even for very small objects. Some examples are light absorbance in infrared (IR) spectroscopy and diffusion in nuclear magnetic resonance (NMR). In IR spectroscopy, absorbance is often calculated based on the oscillator model for polar functional groups. A functional group is not sufficiently small compared to the surrounding objects and analyses based on the Langevin equation may not be justified. Actually, Roy *et al.* [35] measured two-dimensional correlation spectra and reported that the dynamics is not Gaussian. In NMR, diffusion of a proton (or other atom) is estimated from the NMR signal based on a simple diffusion equation for the Brownian motion. (Even if the Langevin equation is not formally justified, we empirically know that the analysis based on the simple Langevin equation gives reasonable results in most cases.) We consider that if the conventional analyses do not give physically reasonable results

we should analyze the data carefully based on the collision dynamics. (Strictly speaking, we should employ quantum dynamics to analyze the IR or NMR data [36]. However, the naive incorporation of Gaussian noise like a Langevin thermostat in quantum systems is questionable [37]. In future work it be useful to consider the modeling of thermostats.)

B. Correlation between collisions

In this section we consider collision events in detail. As we showed, the waiting-time distribution $P(\tau)$ in our system is well described by the exponential distribution. [Assumption (a) in the Burshtein-Krongauz model is not satisfied.] The Burshtein-Krongauz model does not give a negative VAC for the exponential waiting-time distribution. Here it should be mentioned that the exponential waiting-time distribution is also reported for hard-sphere fluids [38]. The reason why the waiting time obeys the exponential distribution is not clear. Because our system is similar to hard-sphere systems in some aspects, we expect there is a common mechanism which gives the exponential waiting-time distribution.

In the Burshtein-Krongauz model, the correlation between the velocities before and after the collision is also an important quantity. To investigate the statistical properties of the collision events in detail, we consider the correlation between velocities by introducing a quantity defined as $\gamma_1 = \langle V' \cdot V \rangle_{\mathrm{coll}} / \langle V^2 \rangle_{\mathrm{coll}}$ (where V and V' are the velocities of the tracer before and after a collision event and $\langle \cdots \rangle_{\mathrm{coll}}$ represents the statistical average with respect to collisions). If we assume that the distribution of the velocity after the collision is Gaussian, the collision event statistics can be characterized only by this γ_1. In the Burshtein-Krongauz model, γ_1 should be negative to give a negative VAC.

It would be informative to analyze γ_1. In our system, the statistics of the fluid particles are simple and thus we can theoretically calculate γ_1, which can be expressed in a simple form as

$$\gamma_1 = \frac{3M}{3M + 4} \qquad (6)$$

(see Appendix B for details of the model and calculations). Here we should note that γ_1 given by Eq. (6) is independent of the ideal-gas density ρ. Therefore, we expect that $\gamma_1 > 0$ holds for any M and ρ. We show the prediction by Eq. (6) together with the simulation data in Fig. 6. We find that Eq. (6) reasonably reproduces the simulation result without any fitting parameters. From these results we conclude that the velocity correlation factor γ_1 cannot be negative in our model. This means that assumption (b) in the Burshtein-Krongauz model is not satisfied either. From these results we conclude that neither assumption in the Burshtein-Krongauz model is satisfied in our system. However, the original idea of the Burshtein-Krongauz model that the dynamics of the tracer is described by the successive collision events seems reasonable. We expect that with several modifications, a Burshtein-Krongauz-type model may explain the dynamical behavior. Before we consider the modification, we should investigate the detailed statistical properties of the collision events.

We consider that the successive collisions can be correlated in our system. Then the correlation factor γ_1 is not sufficient to characterize the properties of the collision events. We
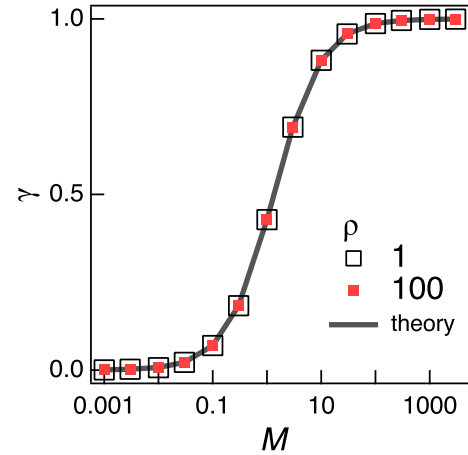

FIG. 6. Correlation factor γ_1 of the velocity before and after a collision. The mass M dependence of γ_1 for two different values of ρ is shown. The data for different ρ are almost the same and data points look fully overlapped.

should investigate multiple collisions which can be correlated. We define the correlation factor for the multiple collision events as

$$\gamma_n \equiv \frac{\langle V_{i+n} \cdot V_i \rangle_{\mathrm{coll}}}{\langle V_i^2 \rangle_{\mathrm{coll}}}. \qquad (7)$$

If the successive collision events are independent, we have $\gamma_n = \gamma_1^n$. If the successive collision events are not statistically independent, γ_n may behave in a different way. Figure 7 shows the correlation factor γ_n directly calculated from the simulations. For $M = 1$ and $\rho = 1$, γ_n decays exponentially as n increases, which seems to be consistent with the estimate based on the statistically independent collisions. For $M = 0.01$ and $\rho = 100$, however, we find that γ_n does not exhibit exponential decay. Clearly, γ_n has a negative peak at $n = 3$, while γ_1 and γ_2 are almost zero. Therefore, the successive collision events are not statistically independent if the mass
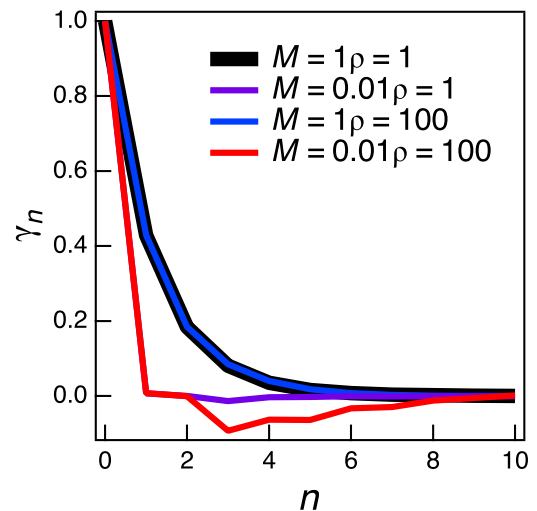

FIG. 7. Correlation factor of the velocity for multiple collisions γ_n. Here n represents the number of collisions. The data for different values of the mass M and the ideal-gas density ρ are shown.

is small and the ideal-gas density is high. As a consequence, we cannot simply apply the Burshtein-Krongauz model.

Based on this result, here we attempt to construct a modified version of the Burshtein-Krongauz model. From the simulation results of the correlation factor data for the multiple collisions γ_n, it would be possible to treat several collision events (for example, $n = 3$ or 4 events) as a coarse-grained event. Then we can express the correlation factor for the coarse-grained collision event as $\gamma_{\mathrm{eff}} = \gamma_n$. Also, the waiting-time distribution between two coarse-grained events becomes

$$
P_{\mathrm{eff}}(\tau) = \int d\tau_1 \cdots d\tau_n \delta(\tau - \tau_1 - \cdots - \tau_n) P(\tau_1) \cdots P(\tau_n)
$$

$$
= \frac{t^{n-1}}{(n-1)!\tau^n} \exp(-\tau/\bar{\tau}). \tag{8}
$$

Equation (8) is the Γ distribution and is clearly different from the exponential distribution, for $n \geqslant 2$. If we assume that coarse-grained collision events are statistically independent, we can utilize the Burshtein-Krongauz model by interpreting their collision events as coarse-grained collision events. With such a coarse graining, the negative velocity correlation can be reasonably explained by the (modified) Burshtein-Krongauz model.

C. Origin of negative correlation

Although the Burshtein-Krongauz model seems to work with some modifications, it does not explain why the correlation factor γ_n becomes negative for $n = 3$. To clarify the emergence mechanism of the negative correlation, we analyze the correlation factor in further detail. Because now we know that the successive collisions are not independent, it would be reasonable to consider whether or not the correlation comes from the same ideal-gas particle. It would be informative to decompose the correlation factor γ_n into the correlation by the collisions with the same ideal-gas particle and the collisions with different ideal-gas particles. We thus define the self- and distinct parts of the correlation factor for multiple collisions:

$$
\gamma_n = \gamma_n^{(s)} + \gamma_n^{(d)}, \tag{9}
$$

$$
\gamma_n^{(s)} \equiv \frac{\langle \mathbf{V}_{i+n} \mathbf{V}_i I(K_{i+1} = K_{i+n}) \rangle}{\langle \mathbf{V}_i^2 \rangle}, \tag{10}
$$

$$
\gamma_n^{(d)} \equiv \frac{\langle \mathbf{V}_{i+n} \mathbf{V}_i I(K_{i+1} \neq K_{i+n}) \rangle}{\langle \mathbf{V}_i^2 \rangle}, \tag{11}
$$

where $I(\cdots)$ takes the value 1 if the argument is true and 0 if not and K_i represents the index of the ideal-gas particle which collides with the tracer at the ith collision event. Figure 8 shows the self- and distinct parts of the collision factor for $M = 0.01$ and $\rho = 100$. From Fig. 8 we find that $\gamma_n^{(s)}$ is negative for $n \geqslant 3$ whereas $\gamma_n^{(d)}$ is positive for all n. This result means that the collisions by different particles do not contribute to the negative correlation and the negative correlation emerges from the collisions with the same particle.

The reason why the correlation occurs at $n = 3$ can be now understood rather intuitively. We consider the sequence of several collision events. At the first collision ($n = 1$), the correlation is always positive ($\gamma_1 > 0$), as we
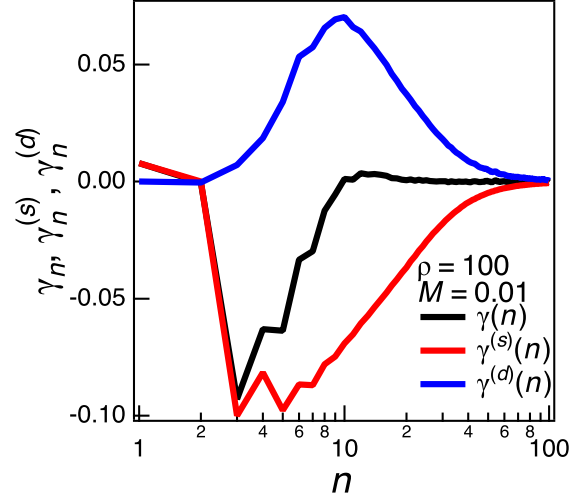

FIG. 8. Self- and distinct parts of the correlation factor for multiple collisions $\gamma_n^{(s)}$ and $\gamma_n^{(d)}$, respectively. The mass and ideal-gas densities are $M = 0.01$ and $\rho = 100$, respectively. The full correlation factor is given as $\gamma_n = \gamma_n^{(s)} + \gamma_n^{(d)}$.

demonstrated. By this first collision, the tracer and the ideal-gas particle exchange momentum and move apart from each other. Therefore, at the second collision ($n = 2$) the tracer cannot collide with the same ideal-gas particle as in the first collision. After the second collision, the momentum of the tracer is changed again and the tracer can move towards the ideal-gas particle which collided in the first collision. Thus, for $n \geqslant 3$, we have the correlation with the same ideal-gas particle.

Before we end this subsection, we briefly discuss the MSD. As is well known, the MSD and the VAC can be related via the Kubo formula [39]. The MSD is obtained by doubly integrating the VAC. Conversely, we have the velocity correlation as

$$
\frac{d^2 \langle \Delta \mathbf{r}^2(t) \rangle}{dt^2} = \langle \mathbf{V}(t) \cdot \mathbf{V}(0) \rangle. \tag{12}
$$

If the velocity correlation becomes negative, at a certain time we should have $\langle \mathbf{V}(t) \cdot \mathbf{V}(0) \rangle = 0$. This means that if we have a negative velocity correlation, we may observe an inflection point in the MSD. In addition, if the negative correlation is strong, the MSD may exhibit an intermediate region between the short-time ballistic region and the long-time diffusive region. Indeed, we observed such a nontrivial intermediate region in Fig. 3(a). Interestingly, the timescale where we observe this intermediate region seems to be the same where we observe the strong peak of the NGP in Fig. 3(b). Therefore, we consider that the collision with the same ideal-gas particle is the origin of various nontrivial short-time behaviors of the tracer.

D. Comparison with other simulations

In this section we compare our results with other simulations. Mizuta *et al.* [20] investigated the dynamics of a single fullerene in liquid argon by using a molecular dynamics simulation. They investigated the dynamics of fullerenes on various timescales. On the short timescale where the time is

shorter than the Enskog time, they showed that the Enskog theory [16] reasonably describes the VAC of a fullerene. The Enskog theory is based on the kinetic theory of gases and thus the results by Mizuta *et al.* imply that the short-timescale dynamics is governed by collisions. The Enskog time is the timescale where approximately only one collision per fluid particle occurs. On longer timescales, the behavior deviates from the Enskog theory. Mizuta *et al.* reported the effect of the fullerene size. For a small fullerene (or for a fluid particle) they reported that the VAC becomes negative in the short-timescale region. This result is qualitatively consistent with ours. However, we should stress that fluid particles strongly interact with each other in their system. Therefore, we cannot quantitatively compare our result with their simulation data. We expect that our analysis would be useful to study some aspects of the short-timescale dynamics in realistic systems like those investigated by Mizuta *et al.*

On a long timescale where the time is longer than the kinematic time of the momentum diffusion over the particle size, they reported that the GLE works reasonably well. Intuitively, on a long timescale, the fluid can be treated as a continuum fluid rather than discrete particles. Then the GLE can be safely employed. This intuitive expectation is consistent with their result. Conversely, our system does not have interactions between the fluid particles and thus it seems unreasonable to treat fluid particles as a continuum fluid. In our system, the fluid particles move ballistically until they collide with the tracer. Because we employed periodic boundary condition, the mean free path λ of the ideal-gas particles depends on the system size as $\lambda \approx \mathcal{V}/\sigma^2$. The Knudsen number Kn can be estimated as follows:

$$\text{Kn} = \frac{\lambda}{\sigma} = \frac{\mathcal{V}}{\sigma^3}. \tag{13}$$

Clearly, the Kn obtained is much larger than 1 for a sufficiently large system (Kn $\gg$ 1). Therefore, we conclude that the ideal gas cannot be regarded as a continuum fluid for the tracer. Consequently, our system does not obey usual continuum hydrodynamic equations such as the Navier-Stokes equation. Our system is designed to study the short-time dynamics and should not be used to study the long-time dynamics. This would explain why we do not observe the long-time tail in the long-time region. To apply the continuum hydrodynamic equations to our model, we should consider very long timescale and very long length scale. The long-time tail may be observed on such a very long timescale, although it would be longer than the current simulation timescale. Because the fluid cannot be expressed by usual continuum hydrodynamic equations, it would not be straightforward to interpret the non-Markovian memory effect in our system. (Normally, the memory kernel can be related to molecular-scale hydrodynamics [11,12,20].) It is not clear whether or not the collision-based description can be successfully related to the hydrodynamic description. It would be an interesting future work to study how the collision-based and hydrodynamic descriptions are connected.

We also compare our results with the simulation by Alder *et al.* [21]. They investigated the effect of the tracer mass and the tracer size on the dynamics in a hard-sphere fluid. They analyzed the VAC of the tracer and showed that the VAC of

the tracer has a negative peak when the mass of the tracer is small. This result is consistent with our result. According to our analysis, such a negative VAC can be attributed to the property of multiple (typically three) sequential collisions. Although the VAC data by Alder *et al.* were not analyzed in terms of collisions, their data seems to be consistent with our analysis: The VAC becomes negative at the time when three collisions occur on average. This implies that our theory holds, at least qualitatively, even with the existence of the hard-sphere interaction between fluid particles. We expect that interpretations and analyses based on collision events will be useful to study the short-time dynamics of various systems.

V. CONCLUSION

We have investigated the short-time dynamics of a tracer in an ideal gas. Our system can be characterized by only two parameters, the mass of the tracer M and the fluid density ρ, in dimensionless units. We performed hard-sphere-type simulations and calculated various dynamical quantities such as the MSD, NGP, and VAC for various values of M and ρ. The dynamical behavior is largely affected by M and ρ. For $M \gtrsim 1$, the NGP is very small and the GLE with Gaussian noise can describe the dynamics well. For $M \lesssim 1$, however, the dynamics cannot be described by a Gaussian stochastic process. We should explicitly consider collision events to describe the dynamics for $M \lesssim 1$. For $\rho \lesssim 1$, the behavior is relatively simple and seems to be consistent with the standard kinetic theory of gases. Meanwhile, for $M \lesssim 1$ and $\rho \gtrsim 1$, some nontrivial dynamical properties have been observed. For example, the VAC exhibits a negative value.

To study the origin of such nontrivial behavior, we analyzed the collision events in detail. We showed that the waiting-time distribution between two successive collisions is almost an exponential distribution and the correlation factor γ_1 is almost positive. The Burshtein-Krongauz model predicts that the VAC is always positive for our system, but it is not consistent with the simulation result. We introduced the correlation factor between multiple collisions γ_n to further investigate the statistical properties of collision events. We showed that the velocities before and after multiple collisions are rather strongly correlated and this correlation is the origin of the negative VAC. In addition, we showed that the strong correlation mainly comes from multiple collisions between the tracer and the same ideal-gas particle.

Although our system is highly idealized and simplified, we believe that our results are informative in the analysis of realistic systems. The dynamical correlation between multiple collision events would exist in realistic systems. Analyses based on the collision picture, such as the analysis of the correlation factor γ_n and the decomposition of it to $\gamma_n^{(s)}$ and $\gamma_n^{(d)}$, would be useful in the analysis of the short-time dynamics in various systems. The analysis of systems with interactions such as the hard-sphere fluid and the Lennard-Jones fluid would be an interesting future work.

APPENDIX A: WAITING-TIME DISTRIBUTION

In this Appendix we roughly estimate the waiting-time distribution for the tracer particle in an ideal gas. The collision statistics depend on the velocity of the tracer relative to an

ideal-gas particle. The distribution of the relative velocity is generally not that simple (as we consider in Appendix B). However, under some special conditions, the distribution reduces to rather simple forms. If the tracer mass is sufficiently large ($M \gg 1$), the tracer velocity becomes very small compared to that of the surrounding ideal-gas particles. The relative velocity distribution approximately coincides with the Maxwell-Boltzmann distribution of the ideal-gas particle. Then the collision statistics do not depend on the tracer velocity V. Individual collision events are expected to be statistically independent and then the number of collisions during a finite-time period should obey the Poisson distribution. This Poisson distribution can be directly related to the exponential waiting-time distribution. Therefore, we expect that the waiting-time distribution becomes exponential if M is sufficiently large.

On the other hand, if the tracer mass is sufficiently small ($M \ll 1$), the relative velocity distribution is almost the same as the tracer velocity V. Here we consider the case where the tracer velocity V is set constant. In this case, the relative velocity distribution is also fixed and we will observe several collision events during a finite-time period. The individual collision events are statistically independent, and thus we expect the exponential waiting-time distribution. Therefore, we have

$$P(\tau|V) = \frac{1}{\bar{\tau}(V)} \exp[-\tau/\bar{\tau}(V)], \qquad (A1)$$

where $\bar{\tau}(V)$ is the average waiting time for the tracer velocity V. We expect that the interval between collisions decreases as the tracer velocity increases. Naively, we consider that the average waiting time can be related to the tracer velocity as $\bar{\tau}(V) = \Lambda/|V|$, where Λ is a mean free path and we assume that Λ is independent of V. (The mean free path Λ depends on the ideal-gas density ρ.) Then we can express the waiting-time distribution as

$$P(\tau) = \int dV \, P(\tau|V) P_{\text{eq}}(V)$$
$$= \int_0^\infty dV \, \frac{V}{\Lambda} \exp(-\tau V/\Lambda) P_{\text{eq}}(V), \qquad (A2)$$

where $V \equiv |V|$, and $P_{\text{eq}}(V)$ and $P_{\text{eq}}(V)$ represent the equilibrium distribution functions for V and V, respectively. The waiting-time distribution can be then calculated to be

$$P(\tau) = \int_0^\infty dV \, \frac{4\pi V^3}{\Lambda} \left(\frac{M}{2\pi}\right)^{3/2} \exp\left(-\frac{\tau V}{\Lambda} - \frac{MV^2}{2}\right)$$
$$= \frac{1}{\Lambda\sqrt{M}} \left[-(3+\tilde{\tau}^2)\tilde{\tau} \exp\left(\frac{\tilde{\tau}^2}{2}\right) \text{erfc}\left(\frac{\tilde{\tau}}{\sqrt{2}}\right)\right.$$
$$\left. + \sqrt{\frac{2}{\pi}}(2+\tilde{\tau}^2)\right], \qquad (A3)$$

with $\tilde{\tau} \equiv \tau/\Lambda\sqrt{M}$. Equation (A3) can be reasonably approximated by the exponential distribution

$$P(\tau) \approx \frac{1}{\Lambda\sqrt{M}} \sqrt{\frac{8}{\pi}} \exp\left(-\sqrt{\frac{8}{\pi}} \frac{\tau}{\Lambda\sqrt{M}}\right). \qquad (A4)$$

Thus, if M is sufficiently small, the waiting-time distribution approximately reduces to the exponential distribution with the average waiting time $\bar{\tau} \approx \Lambda\sqrt{\pi M/8}$.

From the estimates shown above, for both sufficiently large and sufficiently small M cases, we have exponential distributions. For the intermediate M cases, we intuitively expect that the waiting-time distribution would be expressed similarly to Eq. (A3). We replace V by the relative velocity $v' = |V - v|$ (v is the velocity of an ideal-gas particle),

$$P(\tau) = \int_0^\infty dv' \, \frac{v'}{\Lambda} \exp(-\tau v'/\Lambda) P_{\text{eq}}(v'), \qquad (A5)$$

where $P_{\text{eq}}(v')$ is the equilibrium relative velocity distribution. The relative velocity obeys the Maxwell-Boltzmann distribution and thus we approximately have the exponential waiting-time distribution (as in the case of the sufficiently small M). Therefore, the waiting-time distribution will be well approximated by the exponential distribution for any M. This is consistent with the simulation results shown in Fig. 5.

APPENDIX B: CALCULATION OF γ_1

In this Appendix we show a detailed calculation of the correlation factor γ_1. We consider the equilibrium system, in which the ideal-gas particles are distributed uniformly in space, and the velocity is sampled from the Maxwell-Boltzmann distribution.

In what follows, we calculate γ_1 in dimensional units (not in the dimensionless units in the main text) for the sake of clarity. We denote the velocities before and after the collision by V and V'. We denote the velocity of the ideal-gas particle which collides with the tracer by v. We calculate $\gamma_1 = \langle V' \cdot V \rangle_{\text{coll}} / \langle V^2 \rangle_{\text{coll}}$ under the following assumptions.

(i) The ideal-gas particles are uniformly distributed in space.

(ii) Both the tracer and ideal-gas particles obey the Maxwell-Boltzmann distribution

$$P_t(V) = \left(\frac{M}{2\pi k_B T}\right)^{3/2} \exp\left(-\frac{MV^2}{2k_B T}\right), \qquad (B1)$$

$$P_g(v) = \left(\frac{m}{2\pi k_B T}\right)^{3/2} \exp\left(-\frac{mv^2}{2k_B T}\right). \qquad (B2)$$

We consider the velocity of the tracer after the collision with an ideal-gas particle. The velocity after the collision V' is simply obtained from the momentum and the energy conservation

$$V' = V + \frac{2m}{M+m} \hat{r} \cdot (v - V)\hat{r}, \qquad (B3)$$

where $\hat{r}$ is the unit vector between the tracer and the ideal-gas particle when the collision occurs (the direction vector). To calculate γ_1, we need to calculate the ensemble average. We can express the average of the internal product of velocities $\langle V' \cdot V \rangle_{\text{coll}}$ as

$$\langle V' \cdot V \rangle_{\text{coll}} = \frac{\int dV \, dv \, d\hat{r} \, P_t(V) P_g(v) P_d(\hat{r})|v - V| \, V' \cdot V}{\int dV \, dv \, d\hat{r} \, P_t(V) P_g(v) P_d(\hat{r})|v - V|}, \qquad (B4)$$

where $P_d(\hat{\boldsymbol{r}})$ represents the equilibrium distribution of the direction vector. The factor $|\boldsymbol{v} - \boldsymbol{V}|$ comes from the fact that the collision frequency is proportional to the relative velocity between the tracer and the ideal-gas particle. (The average with respect to collision $\langle \cdots \rangle_{\text{coll}}$ is different from the simple equilibrium average by this factor.) From Eqs. (B3) and (B4),

$$\gamma_1 = 1 + \frac{2m}{M+m} \frac{\int d\boldsymbol{V} d\boldsymbol{v} \, d\hat{\boldsymbol{r}} \, P_t(\boldsymbol{V}) P_g(\boldsymbol{v}) P_d(\hat{\boldsymbol{r}}) |\boldsymbol{v} - \boldsymbol{V}| \hat{\boldsymbol{r}} \cdot (\boldsymbol{v} - \boldsymbol{V}) \hat{\boldsymbol{r}} \cdot \boldsymbol{V}}{\int d\boldsymbol{V} d\boldsymbol{v} \, d\hat{\boldsymbol{r}} \, P_t(\boldsymbol{V}) P_g(\boldsymbol{v}) P_d(\hat{\boldsymbol{r}}) |\boldsymbol{v} - \boldsymbol{V}| V^2}. \tag{B5}$$

We can rewrite Eq. (B5) in a simpler form by introducing the reduced mass and the relative velocity. We define $\nu = M + m$, $\mu = Mm/\nu$, $\boldsymbol{u} = (M\boldsymbol{V} + m\boldsymbol{v})/\nu$, and $\boldsymbol{v}' = \boldsymbol{v} - \boldsymbol{V}$. Then Eq. (B5) reduces to

$$\gamma_1 = 1 + \frac{2m}{M+m} \frac{\int d\boldsymbol{u} \, d\boldsymbol{v}' d\hat{\boldsymbol{r}} \, P_d(\hat{\boldsymbol{r}}) |\boldsymbol{v}'| (\hat{\boldsymbol{r}} \cdot \boldsymbol{v}') \hat{\boldsymbol{r}} \cdot (\boldsymbol{u} - \frac{m}{\nu} \boldsymbol{v}') \exp\left(-\frac{\nu \boldsymbol{u}^2 + \mu \boldsymbol{v}'^2}{2k_B T}\right)}{\int d\boldsymbol{u} \, d\boldsymbol{v}' d\hat{\boldsymbol{r}} \, P_d(\hat{\boldsymbol{r}}) |\boldsymbol{v}'| (\boldsymbol{u} - \frac{m}{\nu} \boldsymbol{v}')^2 \exp\left(-\frac{\nu \boldsymbol{u}^2 + \mu \boldsymbol{v}'^2}{2k_B T}\right)}. \tag{B6}$$

We calculate the integral in the denominator of the second term on the right-hand side of Eq. (B6). The integrand does not depend on $\hat{\boldsymbol{r}}$ and thus we can easily perform the integral over $\hat{\boldsymbol{r}}$. Then we have

$$\int d\boldsymbol{u} \, d\boldsymbol{v}' d\hat{\boldsymbol{r}} \, P_d(\hat{\boldsymbol{r}}) |\boldsymbol{v}'| \left(\boldsymbol{u} - \frac{m}{\nu} \boldsymbol{v}'\right)^2 \exp\left(-\frac{\nu \boldsymbol{u}^2 + \mu \boldsymbol{v}'^2}{2k_B T}\right) = \int d\boldsymbol{u} \, d\boldsymbol{v}' |\boldsymbol{v}'| \left(\boldsymbol{u} - \frac{m}{\nu} \boldsymbol{v}'\right)^2 \exp\left(-\frac{\nu \boldsymbol{u}^2 + \mu \boldsymbol{v}'^2}{2k_B T}\right)$$

$$= \pi^{3/2} (2k_B T)^{9/2} \left(\frac{3}{\nu^{5/2} \mu^2} + \frac{4m^2}{\nu^{7/2} \mu^3}\right). \tag{B7}$$

Next we calculate the integral in the numerator of the second term on the right-hand side of Eq. (B6). Without loss of generality, we can set the direction of the relative velocity parallel to the z axis: $\boldsymbol{v}' = [0, 0, v']$. For convenience, we rewrite the direction vector in spherical coordinates as $\hat{\boldsymbol{r}} = [\sin\theta \cos\phi, \sin\theta \sin\phi, \cos\theta]$. To proceed with the calculation, we need the distribution function for the direction vector. Now a collision occurs between the tracer particle fixed at the origin and the ideal-gas particles which moves parallel to the z axis, with velocity v'. Then the distribution of the normal vector should be proportional to the direction vector which is projected onto the xy plane:

$$P_d(\hat{\boldsymbol{r}}_n) \propto |\sin\theta \cos\theta|. \tag{B8}$$

In addition, not all the ideal-gas particles can collide with the tracer. For $v' > 0$, the probability distribution becomes

$$P_d(\theta, \phi) = \begin{cases} -\sin\theta \cos\theta / \pi & \text{for } \pi/2 \leqslant \theta \leqslant \pi \\ 0 & \text{otherwise.} \end{cases} \tag{B9}$$

Similarly, for $v' < 0$, we have

$$P_d(\theta, \phi) = \begin{cases} \sin\theta \cos\theta / \pi & \text{for } 0 \leqslant \theta \leqslant \pi/2 \\ 0 & \text{otherwise.} \end{cases} \tag{B10}$$

By utilizing Eqs. (B9) and (B10), finally we have

$$\int d\boldsymbol{u} \, d\boldsymbol{v}' d\hat{\boldsymbol{r}} \, P_d(\hat{\boldsymbol{r}}) |\boldsymbol{v}'| (\hat{\boldsymbol{r}} \cdot \boldsymbol{v}') \hat{\boldsymbol{r}} \cdot \left(\boldsymbol{u} - \frac{m}{\nu} \boldsymbol{v}'\right) \exp\left(-\frac{\nu \boldsymbol{u}^2 + \mu \boldsymbol{v}'^2}{2k_B T}\right) = -2\pi^{3/2} (2k_B T)^{9/2} \frac{m}{\nu^{5/2} \mu^3}. \tag{B11}$$

By substituting Eqs. (B7) and (B11) into Eq. (B6), we have the following simple expression for γ_1:

$$\gamma_1 = \frac{3M}{3M + 4m}. \tag{B12}$$

This gives Eq. (6). From this derivation, it would be rather trivial that γ_1 does not have a negative value.

[1] R. Brown, Philos. Mag. **4**, 161 (1828).

[2] N. G. van Kampen, *Stochastic Processes in Physics and Chemistry*, 3rd ed. (Elsevier, Amsterdam, 2007).

[3] K. Sekimoto, *Stochastic Energetics*, Lecture Notes in Physics Vol. 799 (Springer, Berlin, 2010).

[4] K. Kawasaki, J. Phys. A: Math. Nucl. Gen. **6**, 1289 (1973).

[5] R. F. Fox, J. Math. Phys. **18**, 2331 (1977).

[6] T. G. Mason and D. A. Weitz, Phys. Rev. Lett. **74**, 1250 (1995).

[7] T. G. Mason, K. Ganesan, J. H. vanZanten, D. Wirtz, and S. C. Kuo, Phys. Rev. Lett. **79**, 3282 (1997).

[8] T. Li, S. Kheifets, D. Medellin, and M. G. Raizen, Science **328**, 1673 (2010).

[9] S. Kheifets, A. Simha, K. Melin, T. Li, and M. G. Raizen, Science **343**, 1493 (2014).

[10] R. Huang, C. Isaac, K. M. Taute, B. Lukić, S. Jeney, M. G. Raizen, and E.-L. Florin, Nat. Phys. **7**, 576 (2011).

[11] D. Lesnicki, R. Vuilleumier, A. Carof, and B. Rotenberg, Phys. Rev. Lett. **116**, 147804 (2016).

[12] A. V. Straube, B. G. Kowalik, R. R. Netz, and F. Höfling, Commun. Phys. **3**, 126 (2020).

[13] J. Patravic, J. Chem. Phys. **129**, 114502 (2008).

[14] N. Kiriushcheva and S. Kuzmin, Physica A **352**, 509 (2005).

[15] T. Yamaguchi and Y. Kimura, J. Chem. Phys. **114**, 3029 (2001).

[16] S. Chapman and T. G. Cowling, *The Mathematical Theory of Non-Uniform Gases: An Account of the Kinetic Theory of Viscosity, Thermal Conduction and Diffusion in Gases*, 3rd ed. (Cambridge University Press, Cambridge, 1990).

[17] A. I. Burshtein and M. V. Krongauz, J. Chem. Phys. **102**, 2881 (1995).

[18] B. Alder and T. Wainwright, Phys. Rev. A **1**, 18 (1970).

[19] P. Herman and B. Alder, J. Chem. Phys. **56**, 987 (1972).

[20] K. Mizuta, Y. Ishii, K. Kim, and N. Matsubayashi, Soft Matter **15**, 4380 (2019).

[21] B. Alder, W. Alley, and J. Dymond, J. Chem. Phys. **61**, 1415 (1974).

[22] O. J. Eder, J. Chem. Phys. **66**, 3866 (1977).

[23] M. F. Gelin, J. Chem. Phys. **141**, 214109 (2014).

[24] M. F. Gelin, A. P. Blokhin, V. A. Tolkachev, and W. Domcke, Chem. Phys. **462**, 35 (2015).

[25] B. J. Alder and T. E. Wainwright, J. Chem. Phys. **31**, 459 (1959).

[26] A. Rahman, Phys. Rev. **136**, A405 (1964).

[27] R. J. Bearman and D. L. Jolly, Mol. Phys. **44**, 665 (1981).

[28] M. J. Nuevo, J. J. Morales, and D. M. Heyes, Phys. Rev. E **51**, 2026 (1995).

[29] W. Kob, C. Donati, S. J. Plimpton, P. H. Poole, and S. C. Glotzer, Phys. Rev. Lett. **79**, 2827 (1997).

[30] C. D. Xue, X. Zheng, K. K. Chen, Y. Tian, and G. Q. Hu, J. Phys. Chem. Lett. **7**, 514 (2016).

[31] F. van Swol and D. N. Petsev, RSC Adv. **4**, 21631 (2014).

[32] T. Ge, G. S. Grest, and M. Rubinstein, Phys. Rev. Lett. **120**, 057801 (2018).

[33] B. M. Vyas, A. V. Orpe, M. Kaushal, and Y. M. Joshi, Soft Matter **12**, 8167 (2016).

[34] A. Malevanets and R. Kapral, J. Chem. Phys. **112**, 7260 (2000).

[35] S. Roy, M. S. Pschenichnikov, and T. L. C. Jansen, J. Phys. Chem. B **115**, 5431 (2011).

[36] Y. Tanimura, J. Phys. Soc. Jpn. **75**, 082001 (2006).

[37] N. G. van Kampen, J. Phys. Chem. B **109**, 21293 (2005).

[38] J. Talbot, Mol. Phys. **75**, 43 (1992).

[39] R. Kubo, Rep. Prog. Phys. **29**, 255 (1966).